RESEARCH ARTICLE

A Modified Variable Switching Frequency Spread-Spectrum PWM Technique With Reduced Torque Ripple for a Vector-Controlled PMSM Drive

MEERA KHALID[1], ANJALY MOHAN[1], (Member, IEEE), PATRICK PAUL PULLUKKARA[1], AND A. C. BINOJKUMAR[2], (Senior Member, IEEE)

[1]Department of Electrical Engineering, Rajiv Gandhi Institute of Technology, Government Engineering College, Kottayam, affiliated to APJ Abdul Kalam Technological University, Kerala 686501, India

[2]Department of Electrical and Electronics Engineering, Government Engineering College Idukki, Idukki, Kerala 685603, India

Corresponding author: Meera Khalid (meerakhalid@rit.ac.in)

ABSTRACT The discrete tonal bands introduced in an AC machine's stator current spectrum by constant switching frequency pulse width modulation schemes, have adverse impacts on the vibration, the acoustic noise, and the electromagnetic interference. Spreading the harmonic spectrum and reducing the magnitude of dominant harmonics is one solution to this problem. Ripples in the electromagnetic torque developed is another major concern in AC drives. Inspired by these factors, this study proposes two novel variable switching frequency schemes for a vector-controlled PMSM drive to disperse the frequency spectrum with a significant reduction in torque ripple. The modulation techniques use linear and trapezoidal variation of sub-cycle sampling period; T_s during their implementation. Further, these methods would be able to eliminate the difficulty in compensator design, which is a major problem with other variable switching frequency schemes. The presented strategies achieve a maximum of 27 % reduction in torque ripple, 51.8 % reduction in dominant harmonics, and a dispersion index of 1.63, demonstrating their competency as promising variable switching frequency schemes. The suggested techniques also show excellent torque ripple reduction capability in comparison with latest spread-spectrum techniques in literature. The proposed techniques are implemented in simulation using MATLAB/Simulink and are experimentally validated using WAVECT-FPGA controller on a 1.07 kW, surface-mounted PMSM drive.

INDEX TERMS PMSM, SVPWM, torque ripple, variable switching frequency PWM, vector control.

I. INTRODUCTION

Permanent Magnet Synchronous motors (PMSM) are promising candidates for Industrial and Electric Vehicle (EV) drives with their features like high efficiency, high torque to weight ratio and compact nature. Excitation of motor phases by non- sinusoidal voltages is the major cause of harmonics in it's stator currents [1], [2], [3]. The authors of [1] have reported that the noise generated by harmonic content in the supply current is greater than those generated

The associate editor coordinating the review of this manuscript and approving it for publication was Feifei Bu[ID].

from imbalance, friction, magnetic sources and aerodynamic reasons. The authors of [4], [5], and [6] have pointed out that constant switching frequency PWM schemes used for AC drives are characterized by concentrated spectral bands in inverter's output voltage leading to increased torque ripple, vibration and acoustic noise at certain frequency bands. The spectral analysis of constant switching frequency PWM schemes shows concentration of harmonics in and around the integral multiples of switching frequency. This has severe impacts on the performance of AC drives.

Generally, the two category of PWM techniques used for spreading the tonal frequency bands are random PWM

schemes and variable switching frequency schemes (VSF). The methods like random PWM, modified random PWM, discontinuous random PWM, and random pulse positioning reported in the literature come under the random PWM category [7], [8], [9], [10], [11], [12], [13], [14], [15], [16], [17], [18]. The random PWM methods explained in [7] and [17] have increased acoustic noise, current ripple and switching loss. This is due to increased concurrent switching and the problem in distributing the zero vector time at high speeds. A randomly varying hysteresis band is used by Chai et al. [19] to implement random switching for acoustic noise reduction. The average switching frequency is high with this method. To improve the spread in spectrum, carrier frequency randomization is adopted in [12], [13], and [16]. This technique utilized random carrier slope or different shapes for modulating signal. But these methods results in poor performance in terms of current ripple though succeeds in achieving spread spectrum. The Latest works on PMSM under harmonic dispersion are done by Pindoriya et al. [20], [21], [22]. Application of random PWM, Pseudo-random PWM and random hysteresis current control technique are studied and its efficacy in spreading spectrum is analysed in these works. These methods have the drawback of increased average switching frequency and high current THD. In all the above-mentioned methods, the switching frequency is random and average switching frequency is not known in advance. This can lead to difficulty in efficiency calculation, designing the thermal subsystem, and the closed loop controller.

It is learned that variable switching frequency schemes have a pre-assigned switching pattern which helps in mitigating the ambiguity regarding the switching frequency. Field Oriented Control (FOC) and Direct Torque Control (DTC) are the two major control strategies for PMSM drives. Performance analysis and characterization of PMSM drives using various control schemes are presented in [23], [24], [25], and [26]. Wang et al. [27] has performed testing of chaotic-SVM based VSF technique on FOC and DTC based systems. The variable frequency PWM schemes employed by [28], [29], [30] achieves reduced inverter switching loss. However current THD tend to increase with these methods. These methods also have increased frequency band and computational complexity. The technique proposed by authors of [31] for induction motors is an effective method for spreading the spectrum with reduced THD and reduced low-order harmonics. But the operating range is low as it is applicable at high modulation indices. It is also found that the current literature on variable frequency schemes have not considered the torque ripple which is an important parameter while designing a PMSM drive.

In-order to address the problems faced by RPWM and VSF schemes, a modified technique is proposed in this work which can spread the harmonic spectrum effectively with reduced torque ripple, good current THD and moderate switching frequency. The major contributions of this study are:

- Stator flux ripple associated with Space Vector PWM (SVPWM) based PMSM drive is analyzed and mathematical models of current and torque ripple are developed.
- A linearly varying sub-cycle sampling period Variable Switching Frequency PWM (VFPWM) is proposed for dispersing the spectrum effectively and reducing the torque ripple.
- A hybrid VFPWM with trapezoidally varying sub-cycle sampling period is developed to further enhance the reduction obtained in torque ripple.
- The suggested techniques are implemented in simulation on a vector-controlled PMSM drive with MATLAB/ Simulink.
- Results obtained in simulation are validated experimentally with WAVECT-FPGA controller on a 1.07 kW PMSM drive.

The intended application of these techniques is medium power industrial drives. The average switching frequency is kept medium, around 6 kHz in this study and it is predeterminable.

The rest of the article is organized as follows. The theoretical background is presented and a torque ripple model is developed in Section II. Implementation of modified spread spectrum techniques are discussed under section III. The Simulation results are presented in section IV and the experimental investigation is presented in Section V. Section VI deals with discussion of the results and performance comparison among the schemes. The concluding remarks are given in section VII.

II. CURRENT RIPPLE, TORQUE RIPPLE AND ACOUSTIC NOISE IN A PMSM

The torque ripple model of a surface-mounted PMSM when operated with Space Vector-based PWM technique is developed by analysing the generated flux ripple. The voltage error resulting from the application of voltage vectors by the inverters for synthesizing a particular reference voltage (V_{ref}) in the space vector modulation technique leads to ripples in stator flux which in-turn leads to current ripple and ripples in the developed torque.

A. STATOR FLUX RIPPLE ASSOCIATED WITH FIXED FREQUENCY PWM INVERTERS

In SVPWM, if an arbitrary instant in a sub-cycle is considered, there is a difference between the applied voltage vector (active or zero voltage vector) and the reference vector which leads to an error voltage. Fig.1 shows the error vectors and the resulting stator flux ripple over a sub-cycle corresponding to the sequence 0-1-2-7 in sector 1. Over a subcycle, the mean square flux ripple can be calculated as follows [32].

$$\tilde{\psi}^2 = \frac{1}{T_s} \int_0^{T_s} \tilde{\psi_q}^2 \, dt + \frac{1}{T_s} \int_0^{T_s} \tilde{\psi_d}^2 \, dt \qquad (1)$$
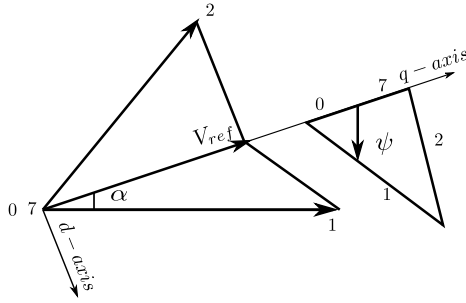
FIGURE 1. Error voltage vectors and the resulting stator flux ripple vector [32].

where $\tilde{\psi}_d$ and $\tilde{\psi}_q$ are the d-axis and q-axis stator flux ripple respectively. This equation is simplified as

$$\tilde{\psi}^2 = \frac{1}{12} T_s^2 V_{ref}^2 + C_1 T_s^2 V_{ref}^3 + C_2 T_s^2 V_{ref}^4 \tag{2}$$

The coefficients C_1 and C_2 are dependent on α; the angle in degrees, between the reference voltage vector (V_{ref}) and the start of the first sector. The d-axis and q-axis flux ripples are separately defined as

$$\tilde{\psi_d}^2 = \frac{1}{3} D^2 \frac{[T_1 + T_2]}{T_s} \tag{3}$$

$$\tilde{\psi_q}^2 = \begin{Bmatrix} \frac{2}{3}(0.5Q_Z)^2 \frac{T_Z}{2T_s} + \frac{1}{3}[(0.5Q_Z)^2 \\ +0.5Q_Z(0.5Q_Z + Q_1) + (0.5Q_Z + Q_1)^2]\frac{T_1}{T_s} \\ +\frac{1}{3}[(0.5Q_Z + Q_1)^2 - (0.5Q_Z + Q_1)0.5Q_Z \\ +(0.5Q_Z)^2]\frac{T_2}{T_s} \end{Bmatrix} \tag{4}$$

where,

$$Q_1 = (cos\alpha - V_{ref})T_1, \quad Q_2 = [cos(60 - \alpha) - V_{ref}]T_2$$
$$Q_Z = -V_{ref}T_Z \quad \text{and} \quad D = sin\alpha T_1 \tag{5}$$

T_1, T_2 and T_Z are the dwell times corresponding to the applied voltage vectors V_1, V_2 and V_0 in sector 1.

$$T_1 = V_{ref} T_s \frac{2}{\sqrt{3}} sin(60 - \alpha) \tag{6}$$

$$T_2 = V_{ref} T_s \frac{2}{\sqrt{3}} sin(\alpha) \tag{7}$$

$$T_z = T_s - (T_1 + T_2). \tag{8}$$

From (2), it is evident that the stator flux ripple in an AC drive depends on V_{ref} (pu), the sub-cycle duration; T_s, and α.

B. TORQUE RIPPLE MODEL OF PMSM

From the small-signal model of PMSM, the stator current ripple arising out of flux ripple due to PWM can be derived. The small-signal model is derived by giving a small perturbation to fundamental d-axis and q-axis voltage equations to account for the ripple quantities in voltages and currents. The resulting current ripple is given by,

$$\tilde{I}_d = \frac{1}{L_d} \int_0^t \tilde{V}_d dt, \quad \tilde{I}_q = \frac{1}{L_q} \int_0^t \tilde{V}_q dt. \tag{9}$$

As the integral of stator voltage ripple is stator flux ripple, the stator current ripple along d-q axis can be defined as,

$$\tilde{I}_d = \frac{\tilde{\psi}_d}{L_d} \quad \text{and} \quad \tilde{I}_q = \frac{\tilde{\psi}_q}{L_q}. \tag{10}$$

Hence, it is followed that the stator current ripple is a function of the PWM inverter-induced stator flux ripple. A model to represent the torque ripple arising out of the current ripple for a surface- mounted PMSM (SPMSM) is presented below. This model establishes the relationship of induced torque ripple with the current ripple and hence with the stator flux ripple. The electromagnetic torque of a PMSM is represented as,

$$T_e = \frac{3}{2} \frac{P}{2}(\psi_d I_q - \psi_q I_d) \tag{11}$$

where, ψ_d, ψ_q and I_d, I_q are the d-q axis flux and current respectively. For an SPMSM, since $L_d = L_q$,

$$T_e = \frac{3}{2} \frac{P}{2} \lambda_f I_q = K_T I_q \tag{12}$$

where, K_T is the torque constant.

Giving small perturbation on both sides, with $\tilde{T}_e$ and $\tilde{I}_q$ representing the ripple in torque and q- axis current respectively of the PMSM,

$$T_e + \tilde{T}_e = K_T(I_q + \tilde{I}_q). \tag{13}$$

Separating the average and the ripple values, the equation for torque ripple becomes,

$$\tilde{T}_e = K_T \tilde{I}_q. \tag{14}$$

Hence, in a surface PMSM, torque ripple is a linear function of q-axis current ripple $\tilde{I}_q$, and $\tilde{I}_q$ itself is a function of stator flux ripple as defined by (10). According to (2), the stator flux ripple in an AC drive depends on V_{ref}, the subcycle duration; T_s, and α.

The pulse width modulation technique used has a significant impact on the acoustic noise generated in AC drives. The sources of acoustic noise in electrical motors fall into three categories. Mechanical, aerodynamic and, electromagnetic. PWM induced noise comes under the electromagnetic noise category. In inverter-fed drives, the fundamental and the time harmonic stator current produces harmonic stator MMF. Electromagnetic forces of different frequencies are generated by the interaction of these airgap fluxes. The major forces are due to the interaction between fundamental and switching frequency fluxes. This electromagnetic force, mainly radial in nature, forces the stator core to vibrate radially. This leads to static deflection of the stator core. The vibration due to the electromagnetic forces results in acoustic noise. The fundamental frequency f varies with speed and the frequency of the radial force gets affected by the changes in speed. If the resultant frequency falls in the neighborhood of the resonant frequency of the motor, it excites resonance and produces vibration and acoustic noise. Otherwise, generally, the acoustic noise generated due to electromagnetic reasons
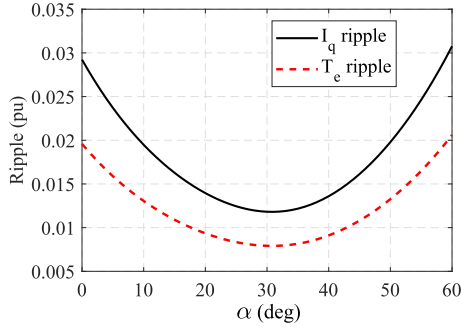
FIGURE 2. The pattern of current and torque ripple for a surface PMSM at $V_{ref} = 0.75$.

FIGURE 3. Proposed Linear variation of T_s within a sector for LISPWM.

does not vary with speed. However, the overall acoustic noise increases with increase in speed owing to the noise contributed from mechanical and aerodynamic reasons. From the above, it is seen that the radial forces and torque ripple are produced due to the interaction between different fluxes. Hence Torque ripple can be considered as indicative of vibration and acoustic noise. The presented study focuses on reduction of torque ripple rather than acoustic noise.

In this paper, the dependency of stator flux ripple and hence the torque ripple on the sub-cycle period; T_s is utilized, to spread out the current harmonic spectrum and to achieve reduced torque ripple for the PMSM drive. Two variable frequency modulation schemes achievable with this logic are explored and detailed in the coming sections.

III. NOVEL SPREAD SPECTRUM TECHNIQUES WITH REDUCED TORQUE RIPPLE

In a surface-mounted PMSM, the torque ripple in the machine is a reflection of the q-axis stator current ripple. A plot of per-unit torque ripple for SPMSM based on (14) is shown in Fig.2, with space vector PWM, where the sub-cycle sampling period; T_s is a constant. The plot is shown for one sector duration and the pattern is identical in other sectors too. The torque ripple has the highest magnitudes at the beginning and the end of the sector ($\alpha = 0°$ and $\alpha = 60°$) and it shows a decreasing tendency towards the middle of the sector i.e., minimum at $\alpha = 30°$. This is the same pattern as that of q-axis current ripple. In-order to minimize the RMS torque ripple, the switching logic developed in this work reduces the torque ripple ($\tilde{T}_e$) at the sectoral ends. $\tilde{T}_e$ is controlled by $\tilde{i}_q$ and $\tilde{\psi}_q$ which is dependent on T_s controls $\tilde{i}_q$. Hence the value of T_s is directly varied to achieve torque ripple reduction at the sectoral ends. The magnitude of T_s is kept minimum (switching frequency maximum) at the sectoral ends and maximum (minimum switching frequency) at the middle. A triangular carrier wave with a variable half-cycle period is used to implement the desired variation in T_s.

Complexity in the controller design is a major challenge with most of the VSF methods. In this work, a simple PWM control strategy is presented where, the controller is easily designed, as the average switching frequency has a pre-assigned value.
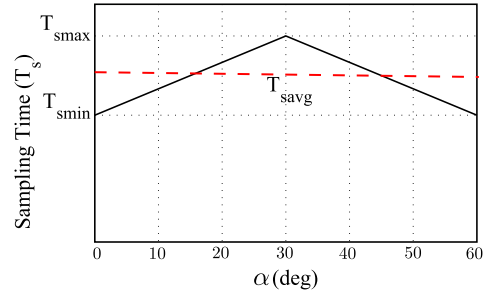
A. LINEAR INVERTED SUB-CYCLE PERIOD PWM (LISPWM)

In the proposed Linear Inverted Sub-cycle period PWM (LISPWM), an inverse linear variation is assigned for T_s to achieve spread spectrum with reduced torque ripple for a PMSM drive. For this, the switching time period of the triangular carrier wave is modified at each half-carrier cycle in accordance with the shape of the torque ripple. Fig.3 shows the variation assigned for T_s with respect to α, in a sector, for the proposed method. It varies between T_{smax} and T_{smin} in a sectoral period. The value of T_s is minimum at the extreme points of a sector, since the torque ripple is maximum at those points. To make the average value of T_s comparable to SVPWM, T_s is designed to be maximum at the middle of the sector. A linear variation is assumed for T_s, as it is easy to implement.

The equations for implementing this scheme are developed from the straight line equations for Fig.3 and are given below.

$$T_s(\alpha) = T_{savg}[1 - K(1 - \frac{2\alpha}{30})], \quad \text{for } 0° \leq \alpha \leq 30°$$
$$= T_{savg}[1 + K(1 - 2\frac{(\alpha - 30)}{30})], \quad \text{for } 30° < \alpha \leq 60°$$

$$(15)$$

where, $T_s(\alpha)$ is the variation in T_s with respect to α. T_{savg} is the average value of T_s over a sector and it is obtained from the area under the T_s curve shown in Fig.3.

$$T_{savg} = \frac{T_{smax} + T_{smin}}{2}. \quad (16)$$

The minimum and maximum periods are defined by using a constant K. Initially T_{smin} is fixed.

$$T_{smin} = T_{savg}(1 - K), \quad T_{smax} = T_{savg}(1 + K). \quad (17)$$

The selection of K depends on factors like the required frequency spread and the low-order harmonics in the stator current spectrum. The value of K can vary between 0 and 1. Lower values of K reduce the dispersion and $K = 0$ corresponds to SVPWM. Higher K values results in increased low-order harmonics and wide variation in the switching frequency of the inverter. Very low values of switching frequency (<1 kHz) may result in motor mechanical resonance. Considering this trade-off, $K = 0.5$ is used in this paper as an optimum value.
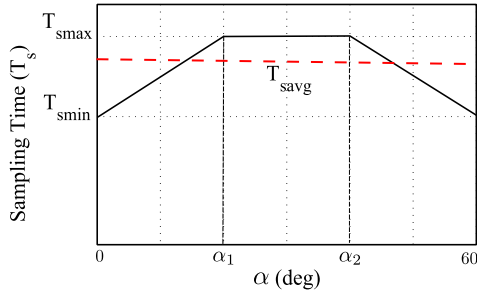
FIGURE 4. Proposed Trapezoidal variation of T_s within a sector for TISPWM.

B. TRAPEZOIDAL INVERTED SUB-CYCLE PERIOD PWM (TISPWM)

In the proposed Trapezoidal Inverted Sub-cycle period PWM (TISPWM) technique, an inverse trapezoidal variation is assigned for T_s as shown in Fig. 4. This is a hybrid modulation strategy comprising of a constant switching frequency part and a variable frequency part. Two variables α_1 and α_2 are defined to fix the boundary between the two parts mentioned above. The angles, α_1 and α_2 are selected symmetrical about the middle of the sector and $\alpha_2 = 60 - \alpha_1$. LISPWM is a special case of TISPWM with $\alpha_1 = \alpha_2 = 30°$. In the presented scheme, T_s has a minimum value (T_{smin}) at $0°$ and $60°$, and is kept at T_{smax} for a duration of α_1 to α_2. A linear variation is assigned for T_s for the rest of the sectoral period. Equations developed for implementing this modulation scheme are shown below.

$$T_s(\alpha) = T_{savg}[\frac{\alpha}{\alpha_1}(1 + K\frac{\alpha_1}{\alpha_2}) + (1 - K)(1 - \frac{\alpha}{\alpha_1})],$$
$$\text{for } 0° \leq \alpha \leq \alpha_1 \quad (18)$$

$$T_s(\alpha) = T_{savg}[1 + K\frac{\alpha_1}{\alpha_2}],$$
$$\text{for } \alpha_1 < \alpha \leq \alpha_2 \quad (19)$$

$$T_s(\alpha) = T_{savg}[(1 - K)(\frac{\alpha - \alpha_2}{\alpha_1})$$
$$+ (1 + K\frac{\alpha_1}{\alpha_2})(1 - (\frac{\alpha - \alpha_2}{\alpha_1}))],$$
$$\text{for } \alpha_2 < \alpha \leq 60°. \quad (20)$$

$$T_{savg} = \frac{\alpha_1 T_{smin} + \alpha_2 T_{smax}}{60}. \quad (21)$$

$$T_{smin} = T_{savg}(1 - K). \quad (22)$$

$$T_{smax} = T_{savg}[1 + K\frac{\alpha_1}{\alpha_2}]. \quad (23)$$

The maximum and minimum periods are defined using K as given in (22) and (23). By properly selecting K, as discussed in the previous section, the proposed technique can be implemented to achieve optimum performance. Here, the value of K is selected as 0.5, which is an optimal value. The control angles α_1 and α_2 are selected as $20°$ and $40°$ respectively.

The minimum switching frequency is kept around 4 kHz in both VSF schemes, in-order to avoid low-order harmonics, while spreading the spectrum. The maximum switching frequency in both cases is 11.2 kHz and the average switching frequency is 5.6 kHz.
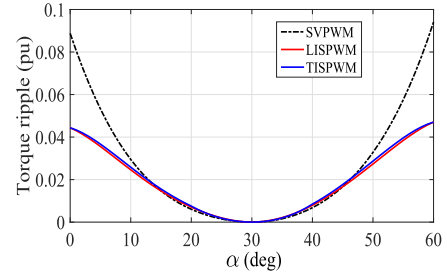

FIGURE 5. Analytical pattern of torque ripple for the constant and variable frequency schemes.

TABLE 1. Parameters of SPMSM.

Symbols	Parameter	Value	Unit
P_{rated}	Power	1.07	kW
N	Rated Speed	4000	rpm
R_s	Stator Resistance	2.2	Ω
L_d	d-axis stator inductance	8.2	mH
L_q	q-axis stator inductance	8.2	mH
P	Number of poles	4	-
λ_f	Permanent Magnet flux	0.226	Wb
J	Moment of inertia	0.000554	Kg.m^2
B	Viscous friction coefficient	0.0043	Nm/rad/s

IV. SIMULATION RESULTS

The pattern of torque ripple obtained analytically for the three schemes is as seen in Fig.5. Significant reduction is seen in instantaneous torque ripple for the VSF schemes as per this analysis. The effectiveness of the proposed VFPWM methods and the correctness of analytical inferences are verified by conducting simulation studies using MATLAB/Simulink. The parameters of the motor used in this study is shown in Table 1. The analysis is carried out under no-load rated-speed condition.

The overall system layout is shown in Fig.6. The entire control consists of vector controller, VSF logic, modulating signal generator, PWM module, and a speed and rotor position estimator. An IGBT based inverter and the motor comprises the power circuit of the system. In vector controller, constant torque angle control is used to maximise the torque developed. For this, the d-axis current is forced to zero. The gains for the closed loop current and speed controllers are designed using symmetric optimum method and are given in Table 2.

The input to the PWM generator is the triangular carrier from the VSF logic, and the modulating signals. Carrier-based approach is used for implementing both SVPWM and VFPWM. The carrier used is a triangular wave with constant/variable sub-cycle duration; T_s, as the case, may be. The α information from the vector controller is processed to implement the VSF logic. $T_s(\alpha)$ is computed from α and T_{savg}, and a triangular carrier with a variable half-cycle period is generated. The average switching frequency used in all the presented schemes is 5.6 kHz. Third harmonic offset is
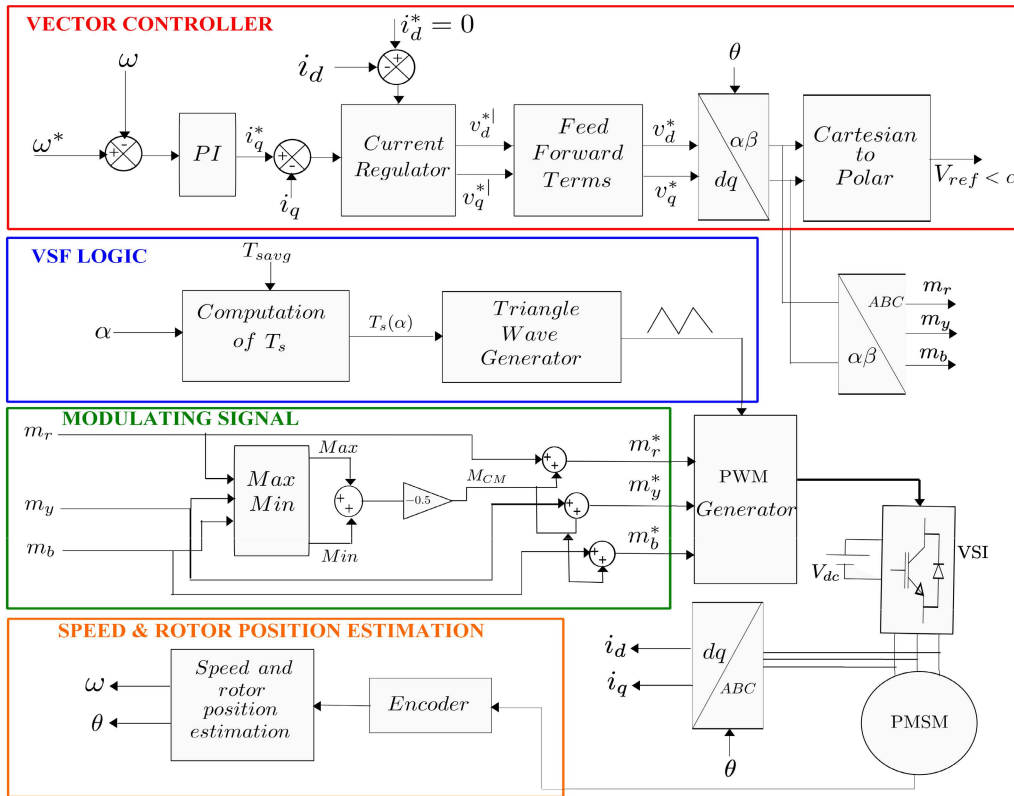
FIGURE 6. Block diagram of vector controlled PMSM drive.

TABLE 2. PI controller parameters.

Controller	K_P	K_I
d-axis current controller	0.366	98.25
q-axis current controller	0.366	98.25
Speed controller	2.34	65.48

added to the three sinusoidal control signals obtained from the vector controller, to form the modulating signals. The PWM generator provides necessary switching signals for the IGBT-based inverter. The speed and rotor position of the motor are estimated from encoder output signals.

Fig.7 shows the results corresponding to inverter fed PMSM drive operated with SVPWM. The d-q axes stator current is shown in Fig.7(a). The ripples in q-axis current, have minimum magnitude at the middle of each sector and relatively higher magnitude towards the ends. The R-phase stator current and it's spectrum are shown in Fig.7(b) and 7(c) respectively. It is seen that the spectrum has harmonic peaks at switching frequency and it's multiples. The dominant harmonic magnitudes are high and have a magnitude of 5% of the fundamental.

The motor is tested under different speed conditions like acceleration, deceleration and reverse speed. This is shown in Fig.7(d). The motor attains steady state speed quickly and runs smoothly under all the speed conditions.

The results corresponding to LISPWM operation are as seen in Fig.8.The reduction of q-axis stator current ripples

at the ends of the sectoral period is seen in Fig.8(a). The spectrum of the R-phase stator current is shown in Fig.8(c). LISPWM has a dispersed spectrum compared to that of SVPWM. The harmonic components spread from 2 kHz to 15 kHz and the magnitude of dominant harmonics is reduced to 4.5% of the fundamental. It is seen that LISPWM achieves comparable current THD as that of SVPWM. The machine operates under all desired speed conditions including reverse speed as seen from Fig.8(d).

The variation in the half cycle period; T_s with α, for the carrier wave used for LISPWM is as shown in Fig.9(a). The carrier wave is shown for one sector duration. It is seen that T_s is a continuously varying function of α and follows the proposed pattern. The triangular carrier generated for the assigned trapezoidal variation of T_s for TISPWM is shown in Fig.9(b). Here, T_s is held constant at T_{smax} around the middle of the sector.

Results obtained under TISPWM operation are shown in Fig.10. This technique also helps to achieve a significant spread in the spectrum as seen from Fig.10(c). In the proposed schemes, it is noted that the current THD is almost comparable to the SVPWM.

The developed electromagnetic torque and it's ripple along with the sector information are shown in Fig.11. In case of SVPWM, as seen from Fig.11(a), the torque ripple has a minimum value at the middle of the sector and reaches maximum at the ends. Fig.11(b) correspond to LISPWM operation in which, the ripple towards the ends of the sector get reduced
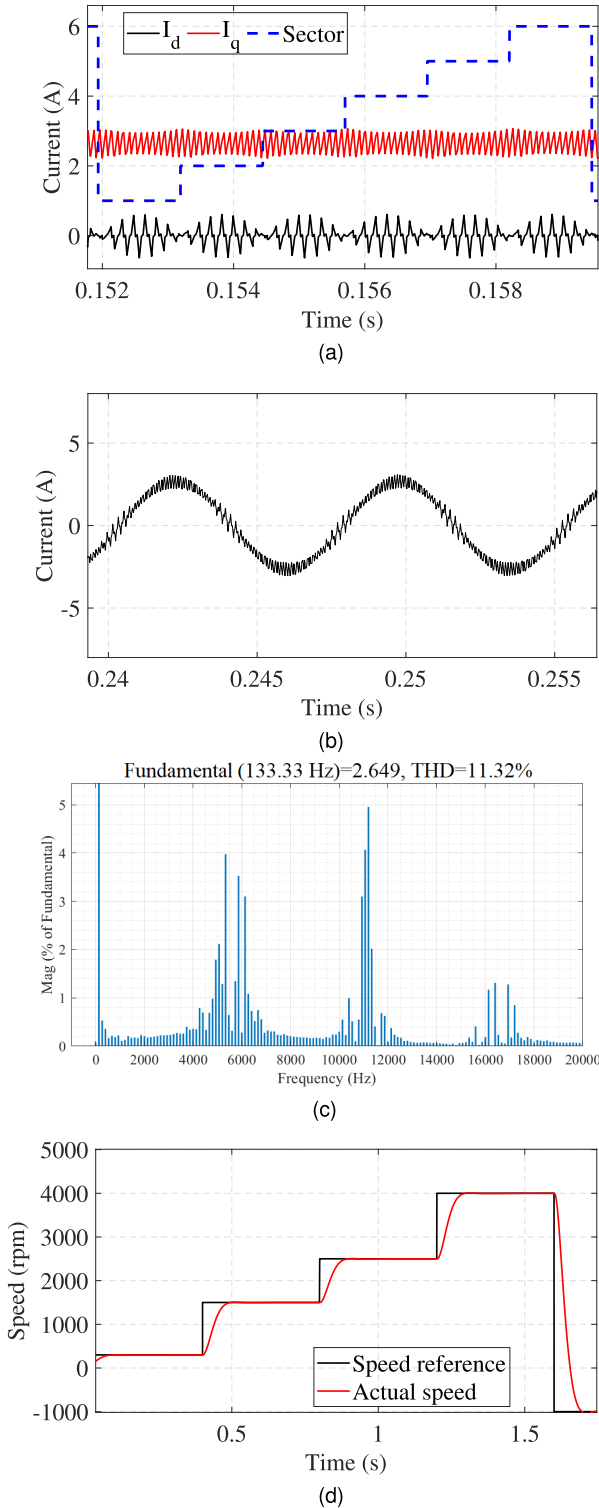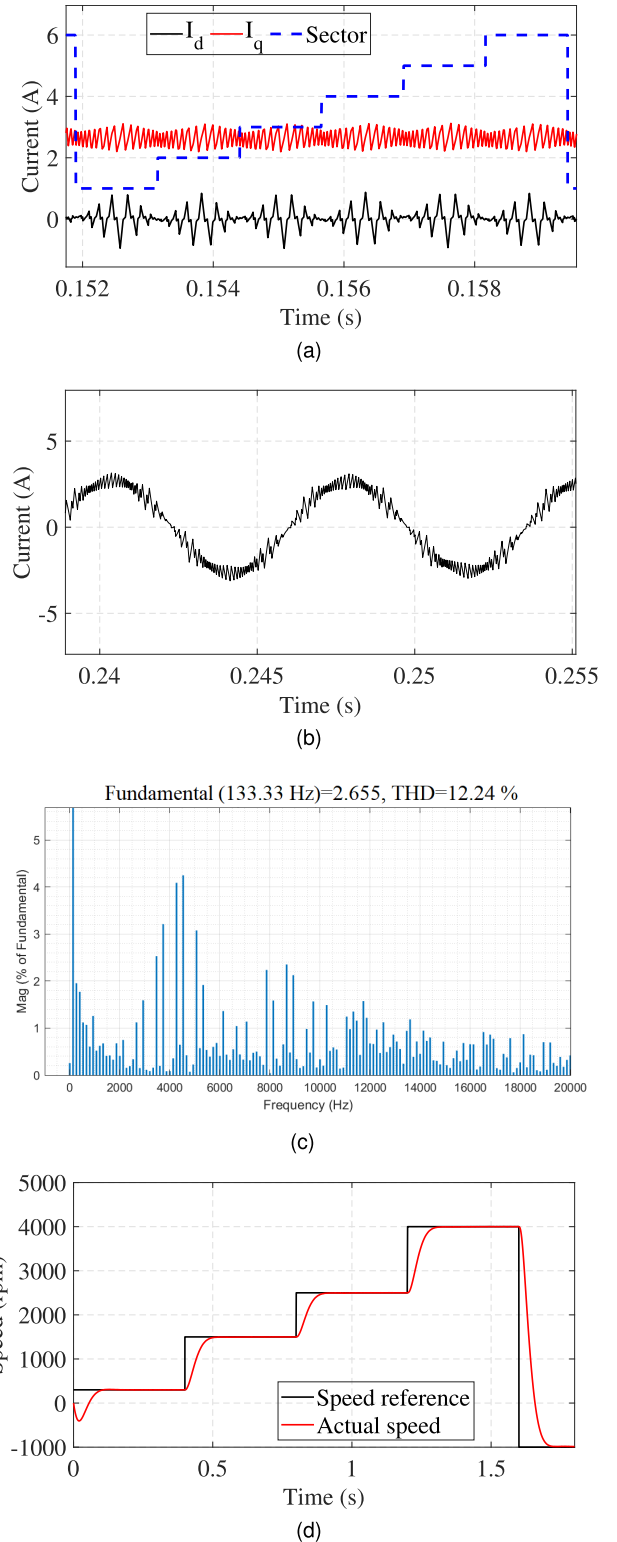
FIGURE 7. Performance of the SPMSM under SVPWM operation (a) *d* and *q* axes stator currents (b) R-phase stator current (c) Stator current spectrum at no-load, rated speed condition (d) Speed of the machine in response to reference speed.

FIGURE 8. Performance of the SPMSM under LISPWM operation (a) *d* and *q* axes stator currents (b) R-phase stator current (c) Stator current spectrum at no-load, rated speed condition (d) Speed of the machine in response to reference speed.

as a result of the applied linear logic, and this results in reduced RMS torque ripple over a sector. The reduction of torque ripple towards the ends of the sector with TISPWM

is clear in Fig.11(c). Here also, the RMS torque ripple in a sector is reduced and is discussed in detail in section VI. Thus, the presented schemes provides excellent performance
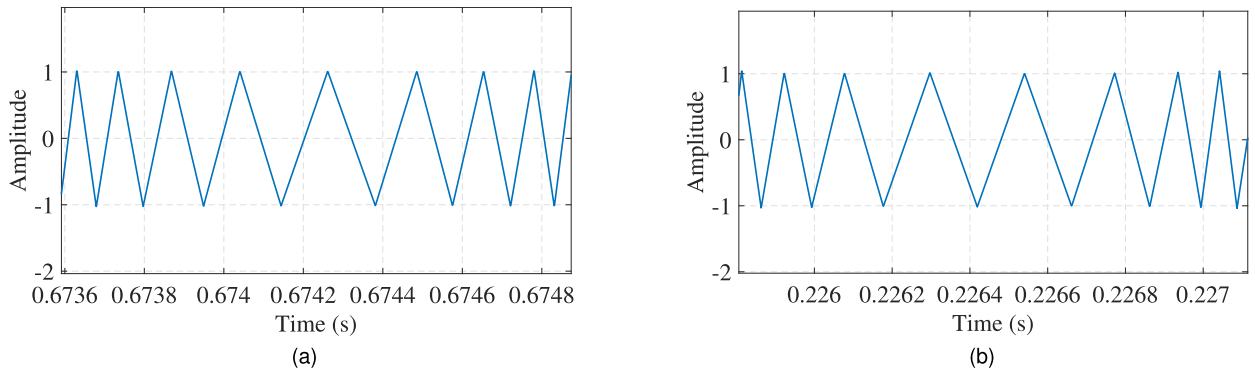
FIGURE 9. Developed triangular carrier in a sector (a) LISPWM (b) TISPWM.
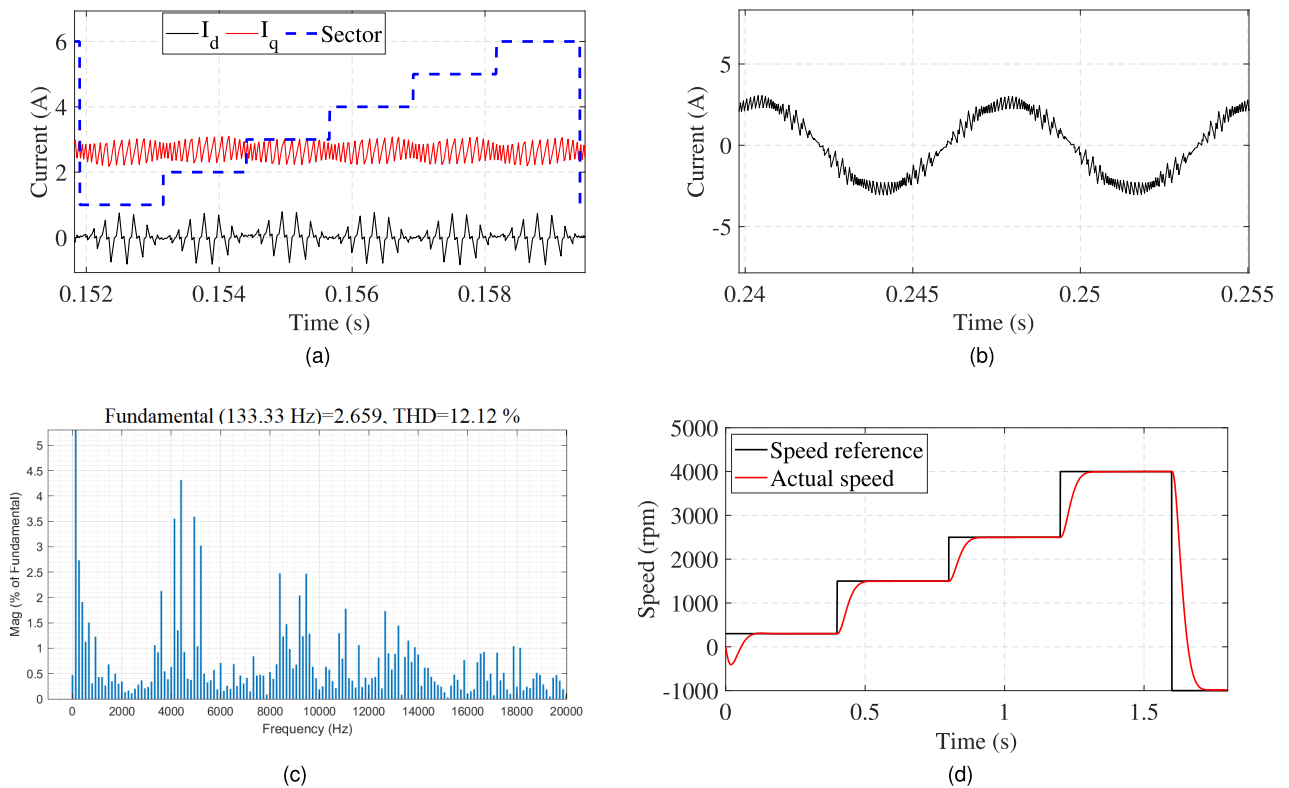

FIGURE 10. Performance of the SPMSM under TISPWM operation (a) d and q axes stator currents (b) R-phase stator current (c) Stator current spectrum at no-load, rated speed condition (d) Speed of the machine in response to reference speed.

in terms of spectrum spread, current THD, speed, and torque ripple.

V. EXPERIMENTAL VALIDATION
The efficacy of the suggested schemes is validated experimentally on a 1.07 kW surface- mounted PMSM drive. The experimental set-up for hardware validation of the results is shown in Fig.12. A 5 kVA, IGBT-based inverter is used to feed the motor. WAVECT-FPGA controller is used as the software platform for implementing the constant frequency and variable frequency PWMs along with vector control. Tektronix TCP312A current probe is used to measure the

stator current. The motor is run under no-load and the performance analysis is carried out in the entire speed region up to 4000 rpm under vector control. Speed and rotor position are estimated from the encoder signals A, B, and Z. The average switching frequency used is 5.6 kHz for all the schemes.

The machine is operated up to it's rated speed of 4000 rpm, starting from a very low speed. The speed dynamics of the PMSM is shown in Fig.13. The actual speed follows the reference speed perfectly with the designed controller values. The variable frequency triangular carriers generated in hardware for LISPWM; the linear VFPWM, and TISPWM; the trapezoidal VFPWM are shown in Fig. 14(a) and 14(b).
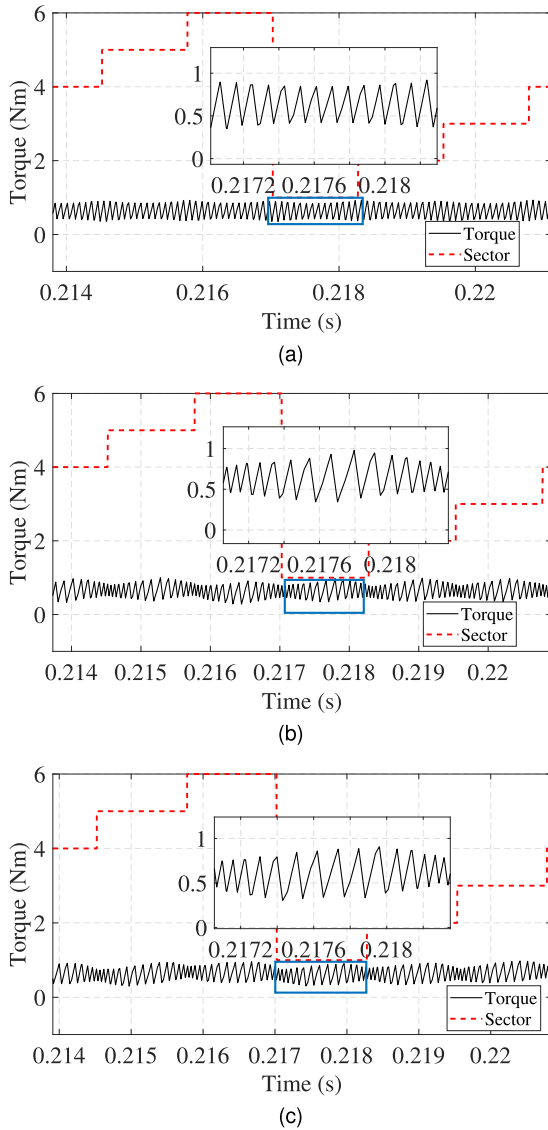
FIGURE 11. Developed electromagnetic torque and it's ripple along with sector information (a) SVPWM (b) LISPWM (c) TISPWM.
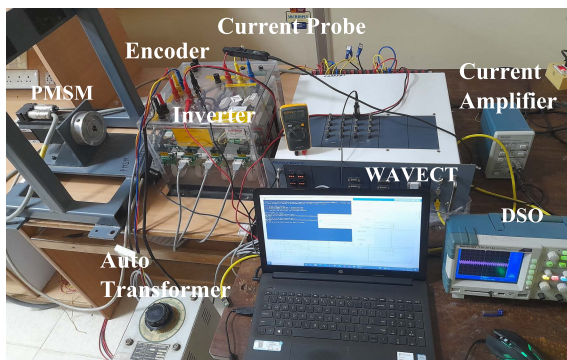

FIGURE 12. Experimental setup of vector controlled PMSM drive with WAVECT controller, IGBT based semikron inverter, current probe and 1.07 kW PMSM.

The triangular carriers have the desired variation in their T_s. Each half cycle period is different for LISPWM and it varies
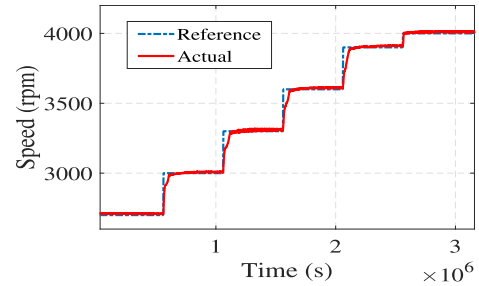

FIGURE 13. Experimentally obtained transient and steady state speed performance of the machine under TISPWM.

with α. For TISPWM, the half cycle period remains constant near the middle of the sector but varying in the rest of the sectoral period.

The shape of d-q axes stator currents and their peculiar pattern within a sector are seen from Fig.15(a) and 15(b). The line voltage V_{RY} and V_{YB} of the inverter are seen in Fig.15(c)corresponding to a DC link voltage 300 V.

Experimentally measured stator current waveforms along with their frequency spectrum are shown for all the schemes in Fig.16. The fundamental current magnitude is approximately 2.6 A (rms) in all cases. The dominant harmonics are decreased with the implemented VSF schemes and sufficient spread in the current spectrum is also obtained. The dispersion in the stator current spectrum starts from 2 kHz. The current THD is almost the same as that of SVPWM at high modulation indices and is within the allowable limits. However, under low-speed regions, the THD is better with SVPWM.

The pattern of torque ripple estimated over a sector from hardware implementation is seen in Fig.17(a)-17(c). The results obtained are in line with the simulation results. The reduction of torque ripple towards the ends of the sector is clearly seen in the proposed VFPWM schemes. This ensures reduced rms torque ripple in a sector.

VI. PERFORMANCE COMPARISON BASED ON SIMULATION AND EXPERIMENTAL RESULTS

An extensive comparison of the VFPWM schemes with SVPWM, based on analytical, simulation as well as hardware results, is provided under different operating conditions. Comparison is carried out in terms of THD of stator current, the magnitude of dominant harmonics, the dispersion index, and the reduction in torque ripple achieved.

The THD of VSF schemes, as already indicated is comparable to SVPWM at high speeds and good dispersion is achieved. The range of spectrum spread obtained is quantified by defining the dispersion index by a new approach that takes into account the ratio of the area occupied by the spectral components of the proposed schemes with that of SVPWM within a chosen frequency band. Following this criterion, the dispersion index obtained for the LISPWM is 1.63 and that of TISPWM is 1.6 with-in a band of 2 kHz to 15 kHz. It is inferred that LISPWM provides a more uniform spread of frequency spectrum compared to TISPWM.
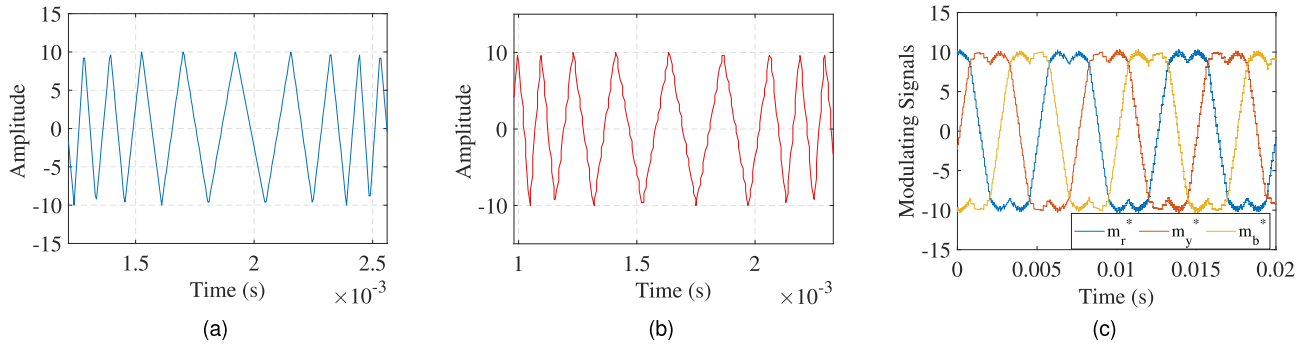
FIGURE 14. Experimentally generated control signals (a) Variable frequency triangular carrier for LISPWM (b) Variable frequency triangular carrier for TISPWM (c) Modulating signals.
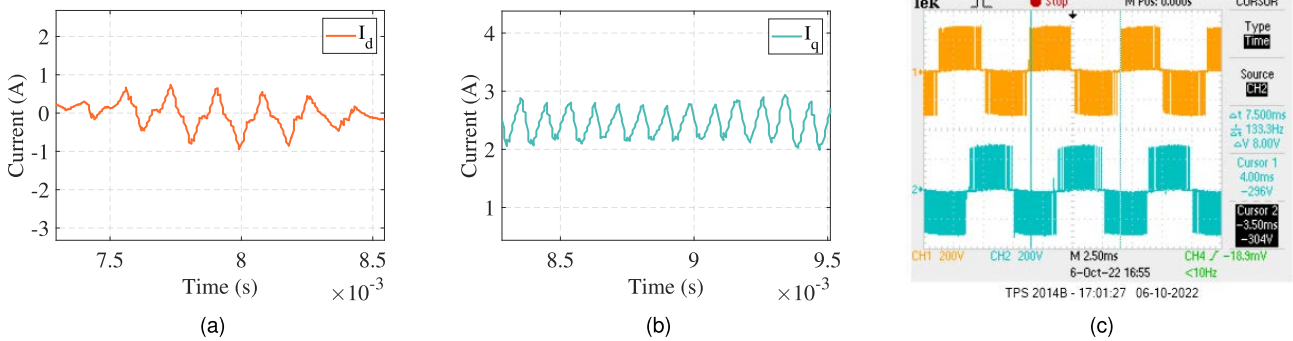

FIGURE 15. (a)-(b) Experimentally measured d-q axes stator currents in one sector with SVPWM (c) Measured line voltages V_{RY} and V_{YB}.
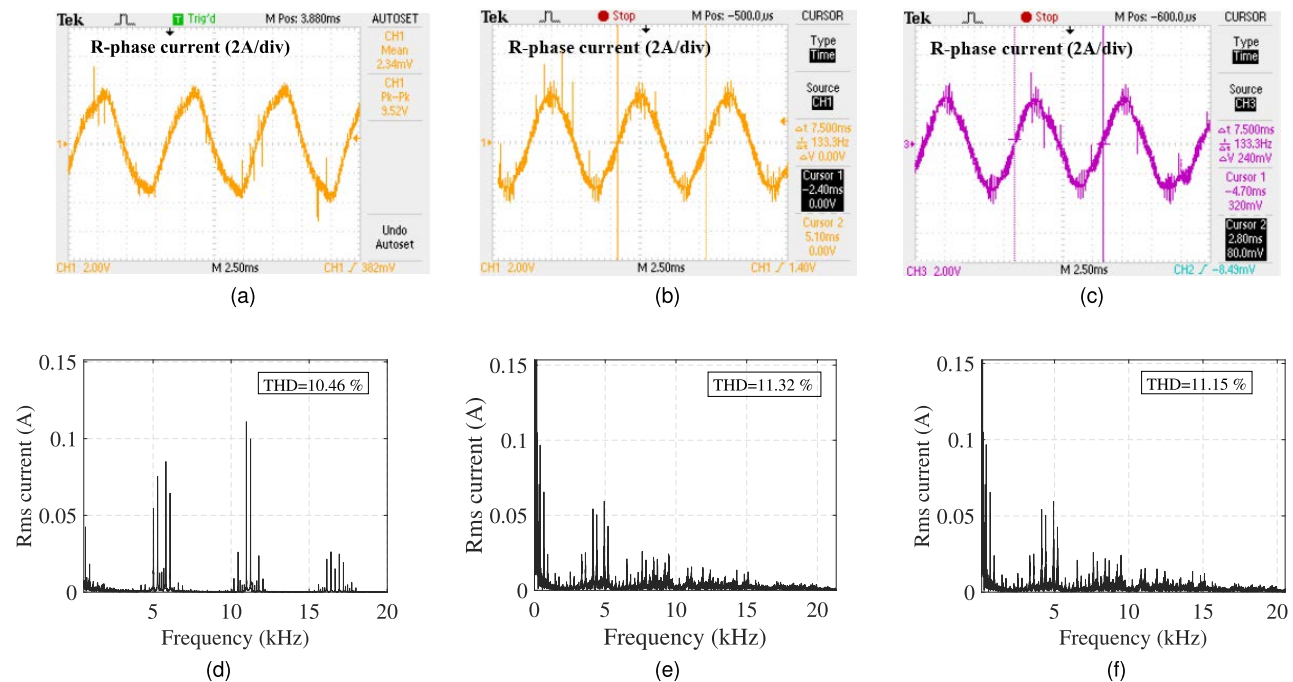

FIGURE 16. (a)-(c)Experimentally measured R-phase stator current for SVPWM, LISPWM, and TISPWM (d)-(f) Experimental stator current frequency spectrum for SVPWM, LISPWM, and TISPWM, at no-load rated speed.

From Fig.18(a), it is observed that dominant harmonics are considerably reduced with the proposed schemes. LISPWM is showing better reduction of dominant harmonics compared to TISPWM. Significant reduction is achieved in torque ripple with VFPWM operation as seen from Fig.18(b) and the percentage reduction achieved with reference to SVPWM
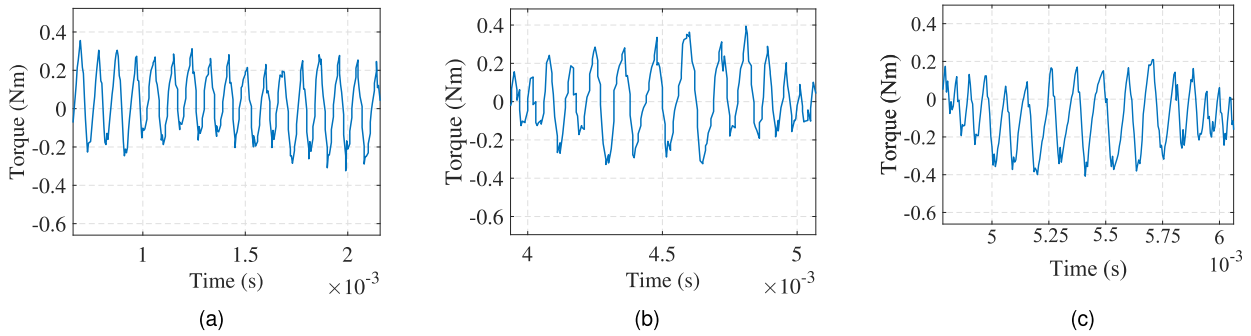
FIGURE 17. (a)-(c) Experimentally measured torque ripple in one sector (a) SVPWM (b) LISPWM (c) TISPWM.
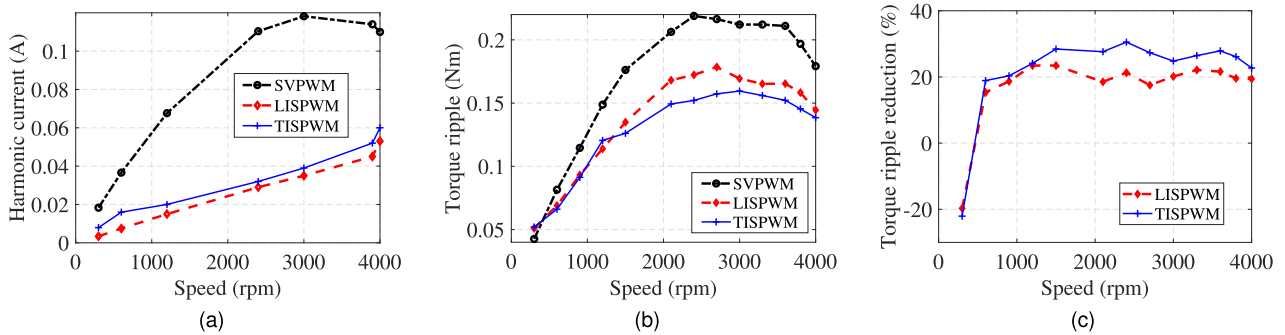

FIGURE 18. Comparison of VFPWM schemes with SVPWM from simulation (a) Dominant Harmonics (b) RMS torque ripple over a sector (c) % reduction in torque ripple.
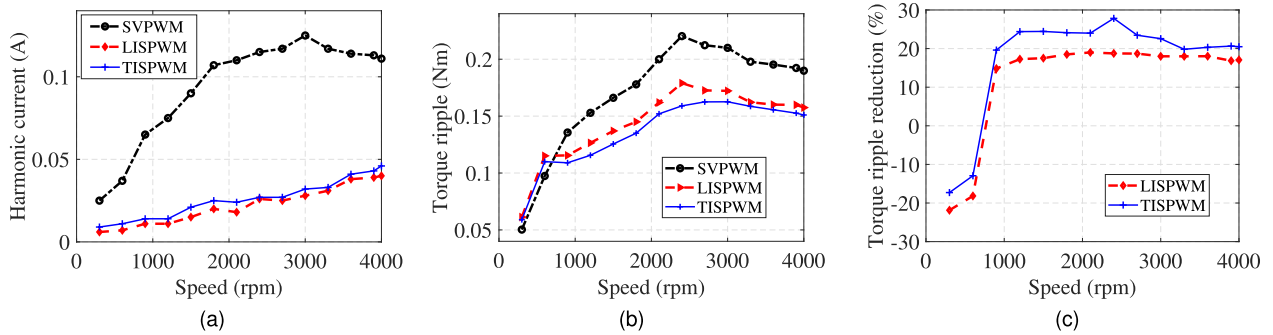

FIGURE 19. Experimental comparison (a) dominant harmonics (b) RMS torque ripple over a sector (c) % reduction in torque ripple.

is quantified in Fig.18(c). It is seen that the ripple in the electromagnetic torque is less with TISPWM compared to LISPWM as the maximum sub-cycle period; T_{smax} is lesser with TISPWM. The results prove the supremacy of the proposed schemes in achieving distributed spectrum with reduced torque ripple, comparable THD, and reduced dominant harmonics when compared to fixed frequency PWM techniques.

An experimental comparison of the dominant harmonics, torque ripple and percentage reduction in torque ripple over the entire speed range, for the three schemes, is given in Fig.19. The results obtained in the experiment match well with the simulation results. In hardware implementation also, the variable frequency schemes effectively spread the spectrum resulting in reduced peaks and reduced dominant

harmonic magnitudes. This is clear in the analysis shown in Figure 19(a), which shows the dominant harmonic current magnitudes. This decrease is 58.3% and 52.6% respectively for the proposed schemes at rated speed. The RMS torque ripple over a sector for the three schemes and the percentage reduction obtained with the VSF schemes is shown in Figs. 19(b) - 19(c). The maximum reduction obtained is 27% with TISPWM and 19% with LISPWM, at high speeds, and at very low speeds, it is negative, meaning SVPWM is having better torque ripple.

The variation of torque ripple with varying speeds is as seen in Fig.20. It increases with speed for all the schemes and after reaching a maximum at around 2500 rpm, it shows a decreasing tendency. This is due to the variation in the pattern of torque ripple with variations in speed. Significant
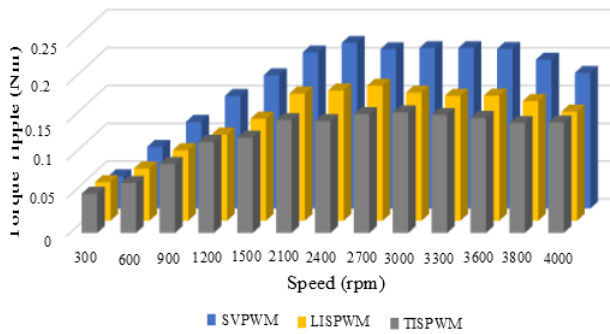
FIGURE 20. Performance in terms of torque ripple.

TABLE 3. Reduction in dominant harmonics and torque ripple compared to SVPWM, at rated speed.

PWM scheme	LISPWM		TISPWM	
	Dominant harmonics reduction (%)	Torque ripple reduction (%)	Dominant harmonics reduction (%)	Torque ripple reduction (%)
Simulation result	51.8	19.4	45.4	22.7
Experimental Result	58.3	17	52.6	20.5

reduction is achieved in torque ripple with VFPWM operation.

A comparison of the results obtained from simulation and hardware is shown in Table 3. The reduction attained in torque ripple during experiment is lesser than that of simulation while dominant harmonics show better reduction during actual testing conditions.

The results corresponding to the proposed modulation techniques are quantified in Table 4. It may be noted that, the frequency range required for TISPWM is less than LISPWM for obtaining the same average switching frequency. Table 5 gives a comparison of the torque ripple of the presented schemes with 3 other spread- spectrum techniques in literature. The results correspond to a speed of 1000 rpm and a load of 1 Nm. For the proposed schemes the switching frequency is 5.6 kHz, whereas, the other schemes included in the table used a frequency of 10 kHz. From the comparison, it is evident that a substantial reduction of torque ripple is achieved with the proposed schemes even with a lesser switching frequency compared to other schemes. This exhibit the excellent torque ripple reduction capability of the proposed methods over it's counterparts. The advantages and limitations of the presented variable frequency modulation techniques are depicted in the chart given in Fig.21. The three schemes are evaluated with respect to different parameters on a 5-point scale. The scale values 0-5 indicates lowest to

TABLE 4. Experimental comparison of the proposed schemes with SVPWM.

Parameter	SVPWM	LISPWM	TISPWM
Switching frequency (kHz)	5.6	5.6 (avg)	5.6 (avg)
Frequency range(Hz)	Constant	3733-11200	4480-11200
Torque ripple at rated speed (Nm)	0.1899	0.1575	0.1510
Reduction in torque ripple at rated speed(%)	-	17	20.5
Highest reduction attained in torque ripple (%)	-	19	27
Dominant Harmonics at rated speed (A)	0.111	0.053	0.06
Reduction in dominant harmonics at rated speed (%)	-	51.8	45.4
Dispersion (Hz)	low	2000-15000	2000-15000
Dispersion Index	1.0	1.63	1.6
THD (at rated speed) %	10.46	11.32	11.15

TABLE 5. Experimental comparison of the torque ripple with other spread-spectrum methods in literature.

Scheme	RHCC-based PWM (f_{sw}=10 kHz, N=1000 rpm) [Ref 20]	PTPWM (f_{sw}=10 kHz, N=1000 rpm) [Ref 22]	RPWM (f_{sw}=10 kHz, N=1000 rpm) [Ref 21]	Proposed LISPWM (f_{sw}=5.6 kHz, N=1000 rpm)	Proposed TISPWM (f_{sw}=5.6 kHz, N=1000 rpm)
Torque ripple (pu)	0.416	0.212	0.122	0.123	0.11

highest with respect to a particular parameter. The reduction in torque ripple, current THD, spread in the stator current spectrum, dispersion index, dominant harmonics, low-order harmonics, switching frequency variation required for getting the same average switching frequency, and easiness of closed-loop controller design are the various criteria selected for analysis. The extensive analysis shows that the proposed modulation techniques excel in majority of the performance criteria, and proves to be promising techniques as VSF-PWM for PMSM drives.
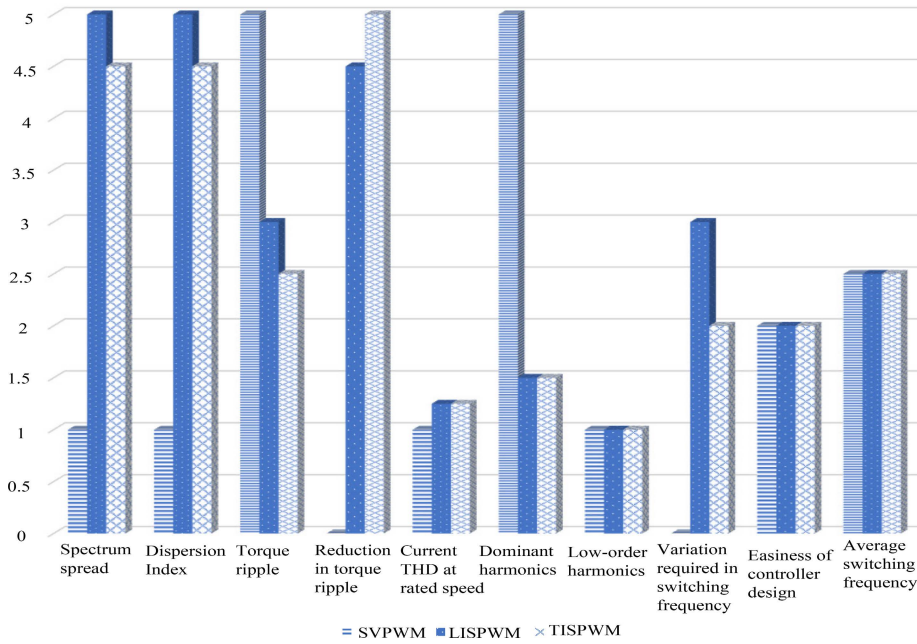
FIGURE 21. Comparison chart depicting various features of the proposed modulation strategy.

VII. CONCLUSION

Two modified variable switching frequency schemes, for dispersing the stator current harmonic spectrum of PMSM drives, with reduced torque ripple, is developed in this work. These methods have reduced torque ripple, a well-dispersed spectrum, and reduced dominant harmonics compared to SVPWM, for a vector-controlled PMSM drive. The results obtained in simulation using MATLAB/Simulink are experimentally validated using FPGA based WAVECT controller on a 1.07 kW PMSM drive. The experimental results obtained are in line with the simulation, and confirm the contributions of the presented study. The torque ripple reduction achieved in experiment, with the proposed methods is 27% and the reduction in dominant harmonics is 51.8 % compared to space vector PWM. The suggested techniques also show excellent torque ripple reduction capability in comparison with latest spread-spectrum techniques in literature. The dispersion index is calculated as 1.63 and 1.6 for the proposed schemes. TISPWM is able to attain higher torque ripple reduction owing to it's hybrid nature. Moreover, it is seen that the suggested techniques do not introduce low-order harmonics and facilitates easier design of compensators compared to other VFPWM schemes. The studies can be extended to interior-type PMSM for EV applications.

A. CONFLICT OF INTEREST

On behalf of all authors, the corresponding author states that the authors have no relevant financial or non-financial interests to disclose.

REFERENCES

[1] R. J. M. Belmans, L. D'Hondt, A. J. Vandenput, and W. Geysen, "Analysis of the audible noise of three-phase squirrel-cage induction motors supplied by inverters," *IEEE Trans. Ind. Appl.*, vol. IA-23, no. 5, pp. 842–847, Sep. 1987.

[2] B. Weilharter, O. Biro, H. Lang, G. Ofner, and S. Rainer, "Validation of a comprehensive analytic noise computation method for induction machines," *IEEE Trans. Ind. Electron.*, vol. 59, no. 5, pp. 2248–2257, May 2012.

[3] D. Franck, M. van der Giet, and K. Hameyer, "Active reduction of audible noise exciting radial force-density waves in induction motors," in *Proc. IEEE Int. Electric Mach. Drives Conf. (IEMDC)*, May 2011, pp. 1213–1218.

[4] W. C. Lo, C. C. Chan, Z. Q. Zhu, L. Xu, D. Howe, and K. T. Chau, "Acoustic noise radiated by PWM-controllel induction machine drives," *IEEE Trans. Ind. Electron.*, vol. 47, no. 4, pp. 880–889, Aug. 2000.

[5] J. Le Besnerais, V. Lanfranchi, M. Hecquet, and P. Brochet, "Characterization and reduction of audible magnetic noise due to PWM supply in induction machines," *IEEE Trans. Ind. Electron.*, vol. 57, no. 4, pp. 1288–1295, Apr. 2010.

[6] A. C. Binojkumar, B. Saritha, and G. Narayanan, "Acoustic noise characterization of space-vector modulated induction motor drives—An experimental approach," *IEEE Trans. Ind. Electron.*, vol. 62, no. 6, pp. 3362–3371, Jun. 2015.

[7] M. M. Bech, F. Blaabjerg, and J. K. Pedersen, "Random modulation techniques with fixed switching frequency for three-phase power converters," *IEEE Trans. Power Electron.*, vol. 15, no. 4, pp. 753–761, Jul. 2000.

[8] A. C. Binojkumar, J. S. S. Prasad, and G. Narayanan, "Experimental investigation on the effect of advanced bus-clamping pulsewidth modulation on motor acoustic noise," *IEEE Trans. Ind. Electron.*, vol. 60, no. 2, pp. 433–439, Feb. 2013.

[9] A. Boudouda, N. Boudjerda, K. E. K. Drissi, and K. Kerroum, "Combined random space vector modulation for a variable speed drive using induction motor," *Electr. Eng.*, vol. 98, no. 1, pp. 1–15, Mar. 2016.

[10] B. Jacob and M. R. Baiju, "Spread spectrum modulation scheme for two-level inverter using vector quantised space vector-based pulse density modulation," *IET Electr. Power Appl.*, vol. 5, no. 7, pp. 589–596, 2011.

[11] H. K. Savadkoohi, D. A. Khaburi, and S. Sadr, "A new switching method for PWM inverter with uniform distribution of output current's spectrum," in *Proc. 6th Power Electron., Drive Syst. Technol. Conf. (PEDSTC)*, Feb. 2015, pp. 242–246.

[12] K. S. Kim, Y. G. Jung, and Y. C. Lim, "A new hybrid random PWM scheme," *IEEE Trans. Power Electron.*, vol. 24, no. 1, pp. 192–200, Jan. 2009.

[13] Y. S. Lai, Y. T. Chang, and B. Y. Chen, "Novel random-switching PWM technique with constant sampling frequency and constant inductor average current for digitally controlled converter," *IEEE Trans. Ind. Electron.*, vol. 60, no. 8, pp. 3126–3135, Aug. 2013.

[14] A. Peyghambari, A. Dastfan, and A. Ahmadyfard, "Strategy for switching period selection in random pulse width modulation to shape the noise spectrum," *IET Power Electron.*, vol. 8, no. 4, pp. 517–523, Apr. 2015.

[15] A. Ruiz-González, M. J. Meco-Gutiérrez, F. Pérez-Hidalgo, F. Vargas-Merino, and J. R. Heredia-Larrubia, "Reducing acoustic noise radiated by inverter-fed induction motors controlled by a new PWM strategy," *IEEE Trans. Ind. Electron.*, vol. 57, no. 1, pp. 228–236, Jan. 2010.

[16] A. Ruiz-Gonzalez, F. Vargas-Merino, J. R. Heredia-Larrubia, M. J. Meco-Gutierrez, and F. Perez-Hidalgo, "Application of slope PWM strategies to reduce acoustic noise radiated by inverter-fed induction motors," *IEEE Trans. Ind. Electron.*, vol. 60, no. 7, pp. 2555–2563, Jul. 2013.

[17] S. E. Schulz and D. L. Kowalewski, "Implementation of variable-delay random PWM for automotive applications," *IEEE Trans. Veh. Technol.*, vol. 56, no. 3, pp. 1427–1433, May 2007.

[18] A. M. Trzynadlowski, F. Blaabjerg, J. K. Pedersen, R. L. Kirlin, and S. Legowski, "Random pulse width modulation techniques for converter-fed drive systems—A review," *IEEE Trans. Ind. Appl.*, vol. 30, no. 5, pp. 1166–1175, Sep./Oct. 1994.

[19] J.-Y. Chai, Y.-H. Ho, Y.-C. Chang, and C.-M. Liaw, "On acoustic-noise-reduction control using random switching technique for switch-mode rectifiers in PMSM drive," *IEEE Trans. Ind. Electron.*, vol. 55, no. 3, pp. 1295–1309, Mar. 2008.

[20] R. M. Pindoriya, A. K. Yadav, B. S. Rajpurohit, and R. Kumar, "A novel application of random hysteresis current control technique for acoustic noise and vibration reduction of PMSM drive," in *Proc. IEEE Ind. Appl. Soc. Annu. Meeting*, Oct. 2020, pp. 1–8.

[21] R. M. Pindoriya, B. S. Rajpurohit, and R. Kumar, "A novel application of harmonics spread spectrum technique for acoustic noise and vibration reduction of PMSM drive," *IEEE Access*, vol. 8, pp. 103273–103284, 2020.

[22] R. M. Pindoriya, G. Gautam, and B. S. Rajpurohit, "A novel application of pseudorandom-based technique for acoustic noise and vibration reduction of PMSM drive," *IEEE Trans. Ind. Appl.*, vol. 56, no. 5, pp. 5511–5522, Sep. 2020.

[23] M. Khalid, A. Mohan, and A. C. Binojkumar, "Performance analysis of vector controlled PMSM drive modulated with sinusoidal PWM and space vector PWM," in *Proc. IEEE Int. Power Renew. Energy Conf.*, Oct. 2020, pp. 1–6.

[24] M. Khalid, A. Mohan, and A. C. Binojkumar, "Evaluation and validation of performance parameters of a permanent magnet synchronous motor drive system with real-time simulator," in *Proc. Int. Conf. Commun., Control Inf. Sci. (ICCISc)*, Jun. 2021, pp. 1–7.

[25] A. Mohan, M. Khalid, and A. Binojkumar, "An investigation into the applications of real-time simulator in experimental validation of PMSM-based electric drive system," in *Advances in Electrical and Computer Technologies*. Singapore: Springer, 2022, pp. 1091–1107.

[26] A. Mohan, M. Khalid, and A. C. Binojkumar, "Performance analysis of permanent magnet synchronous motor under DTC and space vector-based DTC schemes with MTPA control," in *Proc. Int. Conf. Commun., Control Inf. Sci. (ICCISc)*, Jun. 2021, pp. 157–171.

[27] Z. Wang, J. Chen, M. Cheng, and K. T. Chau, "Field-oriented control and direct torque control for paralleled VSIs fed PMSM drives with variable switching frequencies," *IEEE Trans. Power Electron.*, vol. 31, no. 3, pp. 2417–2428, Mar. 2016.

[28] X. Mao, R. Ayyanar, and H. K. Krishnamurthy, "Optimal variable switching frequency scheme for reducing switching loss in single-phase inverters based on time-domain ripple analysis," *IEEE Trans. Power Electron.*, vol. 24, no. 4, pp. 991–1001, Apr. 2009.

[29] W. Cao, F. Wang, and D. Jiang, "Variable switching frequency PWM strategy for inverter switching loss and system noise reduction in electric/hybrid vehicle motor drives," in *Proc. IEEE Appl. Power Electron. Conf. Expo. (APEC)*, Mar. 2013, pp. 773–780.

[30] D. Jiang and F. Wang, "Variable switching frequency PWM for three-phase converters based on current ripple prediction," *IEEE Trans. Power Electron.*, vol. 28, no. 11, pp. 4951–4961, Nov. 2013.

[31] A. C. B. Kumar and G. Narayanan, "Variable-switching frequency PWM technique for induction motor drive to spread acoustic noise spectrum with reduced current ripple," *IEEE Trans. Ind. Appl.*, vol. 52, no. 5, pp. 3927–3938, Sep./Oct. 2016.

[32] G. Narayanan and V. T. Ranganathan, "Analytical evaluation of harmonic distortion in PWM AC drives using the notion of stator flux ripple," *IEEE Trans. Power Electron.*, vol. 20, no. 2, pp. 466–474, Mar. 2005.

MEERA KHALID received the bachelor's degree in electrical and electronics engineering from the Mar Athanacius College of Engineering, Kothamangalam, and the master's degree in industrial drives and control from the Government Engineering College, Rajiv Gandhi Institute of Technology, Kerala, India, in 2003 and 2011, respectively. She is currently pursuing the Ph.D. degree in motor drives and control with the Department of Electrical Engineering, Government Engineering College, Rajiv Gandhi Institute of Technology, Kottayam, under APJ Abdul Kalam Technological University, Thiruvananthapuram, Kerala, India. Her research interests include pulse width modulation techniques and electrical drives.

ANJALY MOHAN (Member, IEEE) received the B.Tech. degree in electrical and electronics engineering from the Saintgits College of Engineering, Mahatma Gandhi University, Kottayam, India, in 2012, and the M.Tech. degree in power electronics and control from the Government Engineering College Idukki, in 2015. She is currently pursuing the Ph.D. degree in motor drives and control with the Rajiv Gandhi Institute of Technology, Kottayam, under APJ Abdul Kalam Technological University, Thiruvananthapuram, India. Her research interests include direct torque control of PMSM and electrical drives.

PATRICK PAUL PULLUKKARA received the bachelor's degree in electrical and electronics engineering from the Sahrdaya College of Engineering and Technology and the master's degree in industrial drives and control from the Government Engineering College, Rajiv Gandhi Institute of Technology, Kottayam, under APJ Abdul Kalam Technological University, Thiruvananthapuram, India. His research interests include motor drives, control designs, and electric vehicles.

A. C. BINOJKUMAR (Senior Member, IEEE) received the B.Tech. degree in electrical and electronics engineering from the Rajiv Gandhi Institute of Technology, Kottayam, India, in 1998, the M.Tech. degree from the College of Engineering, Thiruvananthapuram, India, in 2001, and the Ph.D. degree from the Indian Institute of Science, Bengaluru, India, in 2016. He is currently working as an Associate Professor at the Government Engineering College Idukki, Kerala, India. His research interests include pulse width modulation techniques, electrical drives, and motor acoustic noise.

● ● ●